Let's Roll a BiFTA: Bi-refinement for Fine-grained Text-visual Alignment in Vision-Language Models

Anonymous authors
Paper under double-blind review

Abstract

Recent research has shown that aligning fine-grained text descriptions with localized image patches can significantly improve the zero-shot performance of pre-trained vision-language models (e.g., CLIP). However, we find that both fine-grained text descriptions and localized image patches often contain redundant information, making text-visual alignment less effective. In this paper, we tackle this issue from two perspectives: *view refinement* and *description refinement*, termed as ***Bi**-refinement for **F**ine-grained **T**ext-visual **A**lignment* (BiFTA). *View refinement* removes redundant image patches with high *Intersection over Union* (IoU) ratios, resulting in more distinctive visual samples. *Description refinement* removes redundant text descriptions with high pairwise cosine similarity, ensuring greater diversity in the remaining descriptions. BiFTA achieves superior zero-shot performance on 6 benchmark datasets for both ViT-based and ResNet-based CLIP, justifying the necessity to remove redundant information in visual-text alignment. Our code is available at: `https://anonymous.4open.science/r/BiFTA-TMLR-Re-submission`.

1 Introduction

Drawing from the profound strides made in large-scale pre-training within natural language processing (Radford et al., 2018; 2019; Devlin et al., 2019; Brown et al., 2020), the CLIP model (Radford et al., 2021) aligns vast collections of images with their corresponding natural language captions (e.g., "a photo of a {label}") into a unified embedding space using large datasets. The scaling of the pre-training data in CLIP empowers the model to deliver considerable performance in zero-shot classification (Radford et al., 2021). CLIP performs zero-shot classification by computing cosine similarity scores between image representations and textual label prompts so that the final prediction is determined based on the distribution of these similarity scores (He & Peng, 2017; Liang et al., 2020; Radford et al., 2021). To push the limits of CLIP's zero-shot capabilities, several studies (Menon & Vondrick, 2023; Pratt et al., 2023) leverage the generative capabilities of *Large Language Models (LLMs)* to produce fine-grained, label-specific textual descriptions via prompt templates (e.g., "describe what does a/an {label} look like"). Under this framework, CLIP model computes and integrates the cosine similarity scores between visual representation of the input image and each generated textual descriptions. By enriching the textual modality, these refined prompts significantly boost CLIP's zero-shot classification accuracy. Recently, Li et al. (2024) propose ***w**eighted visual-text **c**ross **a**lignment score* (WCA), which calculates and integrates a weighted cross-alignment score between LLM-generated label-specific descriptions and cropped image patches. By effectively refining the synergy between visual and textual representations, this **cross-alignment scoring** mechanism achieves the *state-of-the-art* (SOTA) zero-shot performance on several downstream tasks.

However, as demonstrated in Figure 1, we observe that both the LLM-generated textual descriptions and the randomly cropped image patches often exhibit redundant content. Such redundancy may introduce disproportionate contributions to the cross-alignment score computation, thereby compromising the accuracy of the resulting alignment. In specific, following WCA (Li et al., 2024), we use random cropping to obtain localized image patches of an image sample (e.g., a border collie), as depicted in Figure 1. We find that these image patches often include certain redundant views exhibiting exceptionally high pairwise cosine similarities (i.e., approaching to 1), which is attributed to the randomness in the cropping method. Similarly,

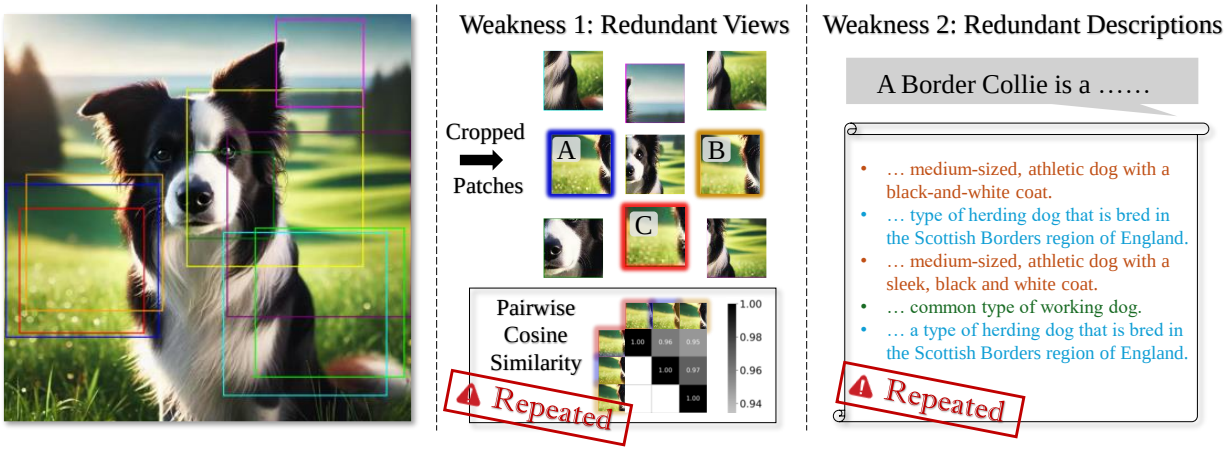

Figure 1: Weaknesses of weighted visual-text cross alignment (Li et al., 2024). **Weakness 1: Pairwise similarity scores of highly overlapping crop bounding boxes.** We demonstrate that image patches A, B, and C, exhibiting significant overlap and redundancy, which provide limited semantic information and consequently contribute minimally to accurate classification. **Weakness 2: Redundant textual descriptions generated by LLM.** We gather textual descriptions from previous work and demonstrate that a significant portion of these descriptions are redundant for a given category, thereby diluting the contribution of meaningful and informative descriptions.

we observe that the diversity of LLM-generated textual descriptions is often restricted by the invariant label-integrated prompt template, which directly leads to generate redundant text responses (see Figure 1). In Figure 2, we further examine how the aforementioned redundancies affect the accuracy of cross-alignment score computation, using the state-of-the-art WCA scoring method as a representative example. We observe from the heatmap that the WCA score corresponding to the ground-truth label becomes more dominant after removing redundant image patches through a simple *Intersection over Union (IoU)* filter. Since the WCA score is computed by aggregating similarity scores between image patches and the textual description, redundant patches introduce repetitive contributions that accumulate disproportionately in the final score. By contrast, after applying IoU filter, the resulting WCA score distribution better aligns with the correct prediction. Furthermore, we find that as the IoU constraint becomes stricter (e.g., IoU $= 0.5$), the accuracy of the WCA score improves correspondingly. These findings suggest that randomly cropping image patches without enforcing overlap constraints may be suboptimal for accurately computing the cross-alignment score. Hence, these observations motivate us to remove redundant information within these image patches and textual descriptions.

To this end, we propose ***Bi**-refinement for **F**ine-grained **T**ext-visual **A**lignment* (BiFTA), a new method to tackle the above-mentioned issue from two perspectives: *view refinement* and *description refinement*. Specifically, *view refinement* uses IoU as the filter metric to efficiently identify and eliminate redundant cropped image patches based on their overlaps of the bounding box. We aim to remove image patches with high IoU ratios, making the remaining visual samples more distinctive. In contrast, *description refinement* first computes the pairwise cosine similarity of the textual descriptions at the representation level, aiming to filter out redundant ones. Then, we select top-k textual descriptions that have the highest cosine similarities with the label caption ("a photo of a/an {label}") from the remaining ones. To better understand BiFTA, we provide theoretical justifications in Section 4.3 to show that our method indeed prioritizes more effective image patches and descriptions while filtering out redundant information.

Through extensive evaluations across six benchmark datasets, we show that BiFTA outperforms baseline methods by notably improving the zero-shot classification accuracy for both ViT-based and ResNet-based CLIP, justifying the necessity to remove redundant information in visual-text alignment. We summarize the main contributions of our work as follows:

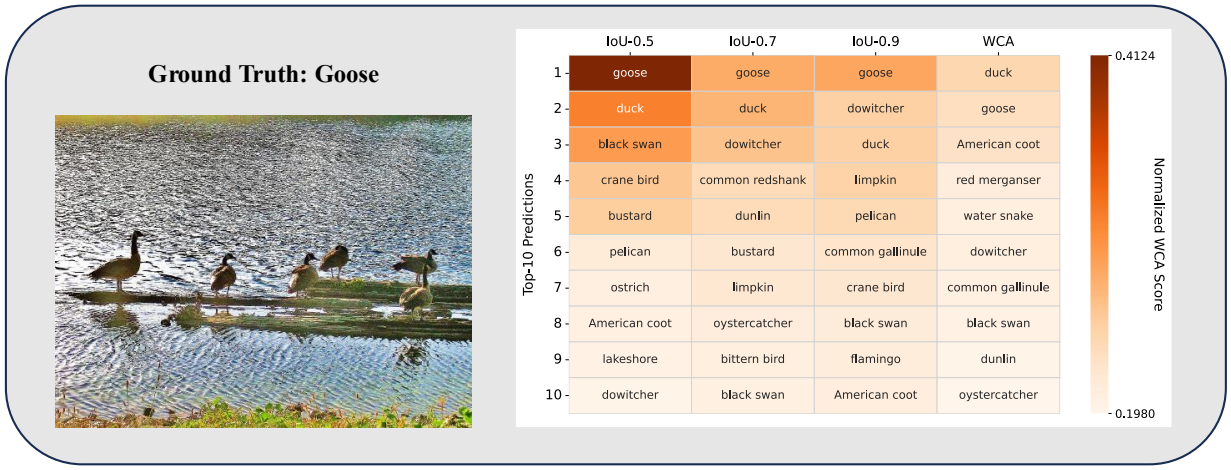

Figure 2: We select an ImageNet image of a goose and display the Top-10 predictions ranked by WCA scores. The scores are normalized using softmax and its distribution is visualized using color intensity. The results show that applying an IoU-based filter to eliminate duplicated image patches significantly enhances the precision of WCA scoring.

- We observe that localized image patches and fine-grained textual descriptions often contain redundant information, making current SOTA visual-text cross-alignment methods less effective.
- We propose an efficient data refinement method, namely BiFTA, to mitigate such redundancy through *view refinement* and *description refinement*, enhancing the alignment between visual and textual modalities.
- We empirically show that BiFTA outperforms baseline methods by achieving significant improvements in zero-shot classification accuracy across 6 benchmark datasets with various CLIP backbones.

2 Related Work

Zero-shot learning for Vision-Language Models. *Vision-language models* (VLMs) have shown their emergent capabilities on image captioning, visual question answering and image classification, which are not specifically pre-trained or explicitly finetuned for these downstream tasks (Radford et al., 2021; Cho et al., 2021; Wang et al., 2021; Kim et al., 2021; Xue et al., 2021; Li et al., 2022a; Alayrac et al., 2022). CLIP (Radford et al., 2021) demonstrates that integrating large-scale pre-training on image-text pairs with a contrastive loss function could enable zero-shot transfer to downstream tasks by simply using natural language prompts. Similarly, ALIGN (Jia et al., 2021) further demonstrates robust representation learning capability of VLMs by pre-training on noisy image-text pairs at large scale. By increasing the scale of the pre-training data and model size, Florence (Yuan et al., 2021) introduces a unified vision-language foundation model capable of zero-shot image classification and retrieval. On the other hand, CoCa (Yu et al., 2022) combines contrastive and generative objectives to improve zero-shot generalization across diverse tasks. The scaling of pre-training data and the contrastive learning paradigm contribute to deeper visual-text alignment and visual understanding of the model.

Textual prompt engineering in VLMs. By scaling the training data, VLMs can learn and understand diverse visual concepts, which can then be transferred to downstream tasks through specific textual label prompting (Radford et al., 2021; Jia et al., 2021; Yuan et al., 2021; Li & Liang, 2021; Singh et al., 2022; Zhou et al., 2022; Shu et al., 2022; Cui et al., 2025). The LLM-integrated textual description generation shows a great generalization ability comparing with existing prompt-learning methods, which often overfit to

training data (Li et al., 2022b; Wang et al., 2022; Wu et al., 2023; Tanwisuth et al., 2023). CLIP (Radford et al., 2021) achieves zero-shot classification by generating classification weights through encoding textual descriptions that uses CLIP template and categories via its text encoder. It then compares these text embeddings with image features extracted by the image encoder to determine the most likely class. Zhou et al. (2022) discover that manually prompt tuning is a time-consuming task and propose CoOp, which models context words with continuous vectors. Subsequently, Menon & Vondrick (2023); Pratt et al. (2023) automatically generates textual category-specific descriptions by leveraging LLMs with different prompt templates. These textual descriptions can accurately reflect visual features of images in each category. More recently, *retrieval-augmented generation* (RAG) is proposed to help to generate accurate descriptions of categories, which is a training-free framework that can be directly integrated during inference time (Yu et al., 2024; Chan et al., 2024; Guo et al., 2024). It retrieves semantically relevant documents by computing embedding vector similarity and provides the retrieved information as supplementary context to LLMs, enabling more accurate and informed responses.

Fine-grained visual-text alignment. *Weighted visual-text cross alignment* (WCA) (Li et al., 2024) has done empirical observation on the embedding alignment between visual patches and textual descriptions. It uses random crops to augment image samples and utilizes cosine similarity to extract informative patches. Similarly, it utilizes distinctive textual descriptions from LLM to cross-align with the image patches. There are uncertainties when cropping samples randomly, and the textual descriptions are not corresponding to fine-grained image patches. AttrVR (Cai et al., 2025) uses descriptive and distinctive attributes of each categories from LLM outputs. In our method, we augment the textual descriptions by integrating various description generation methods to further select the high-quality textual descriptions.

3 Preliminary

CLIP Zero-shot Classification. CLIP (Radford et al., 2021) is a pre-trained VLM that consists of a text encoder $f_{\text{txt}} : \mathcal{T} \to \mathcal{Z}$ and an image encoder $f_{\text{img}} : \mathcal{X} \to \mathcal{Z}$, where $\mathcal{T}$ is a discrete text space, $\mathcal{X}$ is a continuous image space and $\mathcal{Z} \subseteq \mathbb{R}^n$ is a shared n-dimensional embedding space. These encoders take an image $X \in \mathcal{X}$ and a text $T \in \mathcal{T}$ as input pair (X, T), mapping them into the shared latent space $\mathcal{Z}$. Then the similarity score between the image and text embedding is calculated as:

$$\text{sim}_{\text{CLIP}}(X, T) = \cos\left(Z_i, Z_t\right)/\tau, \text{ with } Z_i = f_{\text{img}}(X), \text{ and } Z_t = f_{\text{txt}}(T),$$

where $\cos(\cdot, \cdot)$ denotes the cosine similarity such that $\cos(Z_i, Z_t) = \frac{Z_i \cdot Z_t}{\|Z_i\|\|Z_t\|}$ and τ is a temperature parameter.

For downstream classification tasks, the text encoder of CLIP model receives a label prompt string $\hat{T}_y$ (e.g., "This is a photo of a/an [y]"), where $y \in \mathcal{Y}$. Subsequently, CLIP model predicts the label which maximizes the probability of $p_{\text{CLIP}}(Y|X)$, given by:

$$\arg\max_{y \in \mathcal{Y}} p_{\text{CLIP}}(Y = y \mid X) = \frac{\exp\left(\text{sim}_{\text{CLIP}}(X, \hat{T}_y)\right)}{\sum_{y' \in \mathcal{Y}} \exp\left(\text{sim}_{\text{CLIP}}(X, \hat{T}_{y'})\right)}.$$

Here, the label y that maximizes the conditional probability $p_{\text{CLIP}}(Y = y \mid X)$ will be chosen, where the visual and textual representations exhibit the highest similarity within the embedding space $\mathcal{Z}$. This enables zero-shot classification capability on CLIP model, as it can generalize to unseen categories without additional fine-tuning.

Weighted Cross-Alignment (WCA). WCA is a scoring method specifically designed to improve the visual-text cross-alignment capability of the CLIP model (Li et al., 2024). First, an original image $X = x$ is randomly cropped with a window size ranging from $[\alpha, \beta] \in [0, 1]$ for n times. It obtain n cropped image patches denote as $I_i = \text{rnd_crop}(x), i \in [0, n]$, where $\text{rnd_crop}(\cdot)$ is the random cropping function that obtains localized visual features (Li et al., 2024). On the other hand, WCA would prepare m textual descriptions $T_1, T_2, ..., T_m$ generated by LLMs, which encompass descriptive features of each category $y \in \mathcal{Y}$. The textual descriptions are collected by leveraging a LLM with manually crafted prompt templates, such as

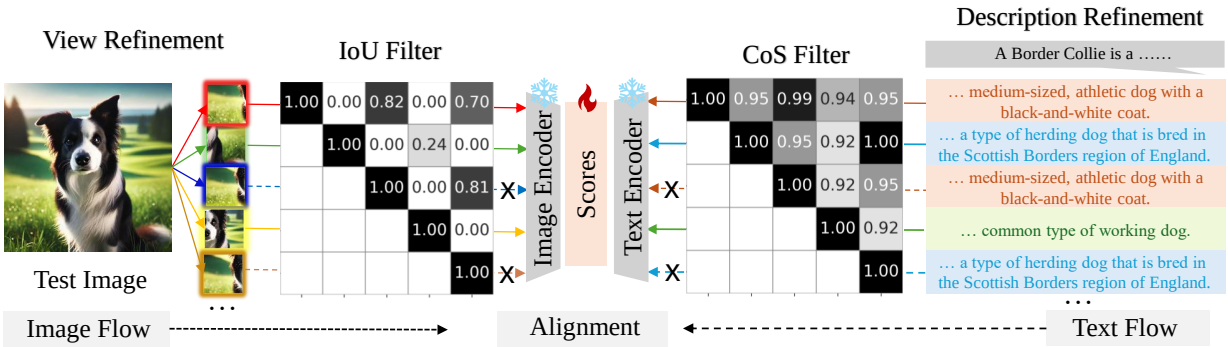

Figure 3: **An Overview of BiFTA.** To reduce potential redundancy in views and descriptions, the randomly cropped views undergo filtering with the IoU filter (Section 4.1), while the randomly sampled description texts are processed using the CoS filter (Section 4.2) when computing the similarity between a single image and a single label. The similarity score is then calculated on the refined views and descriptions.

"Describe what a/an category looks like." (Pratt et al., 2023). Then the visual-text similarity score matrix can be presented as:

$$\begin{bmatrix} \mathrm{sim}_{\mathrm{CLIP}}(I_1, T_1) & \cdots & \mathrm{sim}_{\mathrm{CLIP}}(I_1, T_m) \\ \vdots & \ddots & \vdots \\ \mathrm{sim}_{\mathrm{CLIP}}(I_n, T_1) & \cdots & \mathrm{sim}_{\mathrm{CLIP}}(I_n, T_m) \end{bmatrix},$$

where $\mathrm{sim}_{\mathrm{CLIP}}(I_i, T_j)$ represents the similarity scores between a specific textual description T_j and an image patches I_i. When applying WCA, the overall similarity score between image x and label y is as follows:

$$\mathrm{sim}_{\mathrm{WCA}}(X = x, Y = y) = \sum_{i=1}^{n} \sum_{j=1}^{m} w_i v_j \mathrm{sim}_{\mathrm{CLIP}}(I_i, T_j), \tag{1}$$

where w_i and v_j are weights for image patch I_i and textual description T_j, respectively. They are obtained from the similarity between I_i and the original image x, or T_j and the label prompt string $\hat{T}_y$, i.e., $w_i = \mathrm{softmax}(\cos(f_{\mathrm{img}}(x), f_{\mathrm{img}}(I_i)))$ and $v_j = \mathrm{softmax}(\cos(f_{\mathrm{txt}}(\hat{T}_y), f_{\mathrm{txt}}(T_j)))$. WCA effectively aligns visual-text pairs with aforementioned weights (Li et al., 2024). However, redundant information may appear in image patches and textual descriptions, leading to the weaknesses shown in Figure 1.

4 BiFTA: View Refinement and Description Refinement

The BiFTA framework seeks to eliminate redundant information from two primary perspectives: (1) view refinement (Section 4.1), which removes overlapping image patches based on IoU scores; and (2) description refinement (Section 4.2), which integrates multiple methods for generating fine-grained textual descriptions and filters semantically similar embeddings using cosine similarity scores. An overview of BiFTA is illustrated in Figure 3. Our approach integrates efficient data filtering and refinement techniques to refine cross-aligned image-text pairs, ultimately enhancing the quality and accuracy of image classification. Furthermore, in Section 4.3, we mathematically prove that BiFTA generates more effective views and descriptions by leveraging posterior probability analysis.

4.1 View Refinement

As shown in Section 3, in WCA, for a single image x, a set of randomly cropped image patches $V = \{I_1, I_2, ..., I_n\}$ is created for subsequent cross-alignment. However, as illustrated in Figure 1, the random cropping method frequently selects the same region or adjacent regions for cropping, which could affect the classification results. Therefore, without changing the size of the set $|V|$, we make $|V|$ into a queue to store

all the image patches. Then we employ a filtering function $f_{\text{IoU}}(\cdot)$ to ensure that each newly cropped image patch added to the current V does not have excessive overlap areas with the existing images in current queue. For a newly cropped image $I_i = \text{rnd_crop}(x)$, the filtering function can be expressed as:

$$f_{\text{IoU}}(I_i, V) = \begin{cases} 1 & \forall I \in V, \text{IoU}(I, I_i) < 1 - \delta \\ 0 & \exists I \in V, \text{IoU}(I, I_i) \geq 1 - \delta \end{cases}, \tag{2}$$

where IoU(.) is the Jaccard index[1] (i.e., intersection over union) between two image patches, and $1 - \delta$ is a hyperparameter representing the IoU threshold detailed in Section 5. When $f_{\text{IoU}}(I_i, V) = 0$, the view set V remains unchanged. However, if $f_{\text{IoU}}(I_i, V) = 1$, V will be appended with the new view I_i, i.e., $V \leftarrow V \cup \{I_i\}$. Thus, by maintaining the size of V consistent with WCA, our method effectively introduces a greater number of semantically independent views.

4.2 Description Refinement

In previous works, CuPL (Pratt et al., 2023) used label-integrated prompt templates such as "Describe what a/an [label] looks like" to obtain various appearance descriptions of different classes. Meanwhile, AttrVR (Cai et al., 2025) employs prompts like "Describe the appearance of [task] [label]" to obtain DesAttr (which describes intra-class features) and DistAttr (which distinguishes inter-class features). Here, we take the union of the descriptions obtained by these methods as the preliminary refinement data.

For a given label y, let us denote the three sets of descriptions as $T^{\text{CuPL}}(y), T^{\text{Des}}(y), T^{\text{Dist}}(y)$, respectively. We can then formulate the equation as:

$$T^{\text{CuPL}}(y) = f_{\text{LLM}}(y|[\text{cupl_prompt}]), T^{\text{Des}}(y) = f_{\text{LLM}}(y|[\text{des_prompt}]), T^{\text{Dist}}(y) = f_{\text{LLM}}(y|[\text{dist_prompt}]),$$

where $f_{\text{LLM}}(\cdot)$ returns the LLM output given queries, and $\text{cupl_prompt}, \text{des_prompt}, \text{dist_prompt}$ are aforementioned prompts used by these methods.

Similar to the *view refinement*, in order to alleviate the redundancy when obtaining description set $D = \{T_1, T_2, ..., T_m\}$, we also employ a filtering function $f_{\text{CoS}}(\cdot, \cdot)$ during random sampling. When sampling text $T_i \in T^{\text{CuPL}}(y) \cup T^{\text{Des}}(y) \cup T^{\text{Dist}}(y)$, the filter function $f_{\text{CoS}}(T_i, D)$–which determines whether new sampled T_i should be included in current set D–can be represented as $f_{\text{CoS}}(T_i, D) = f_{\text{CS}}(T_i, D) \cdot f_{\text{TopK}}(T_i, D)$, which consists of a filter $f_{\text{CS}}(\cdot, \cdot)$ that removes similar descriptions:

$$f_{\text{CS}}(T_i, D) = \begin{cases} 1 & \forall T \in D, \cos(f_{\text{txt}}(T), f_{\text{txt}}(T_i)) < 1 - \epsilon \\ 0 & \exists T \in D, \cos(f_{\text{txt}}(T), f_{\text{txt}}(T_i)) \geq 1 - \epsilon \end{cases},$$

and another filter $f_{\text{TopK}}(\cdot, \cdot)$ for eliminating noisy or irrelevant descriptions:

$$f_{\text{TopK}}(T_i, D) = \begin{cases} 1 & T_i \in \text{Top-K}(\cos(f_{\text{txt}}(\hat{T}_y), f_{\text{txt}}(T))|T \in D) \\ 0 & T_i \notin \text{Top-K}(\cos(f_{\text{txt}}(\hat{T}_y), f_{\text{txt}}(T))|T \in D) \end{cases},$$

where ϵ is a hyperparameter representing the threshold, Top-K$(\cdot)$ returns the set of variable Ts corresponding to the top k function values, and $\hat{T}_y$ is the label prompt string (e.g. "This is a photo of a/an [label]").

The use of $f_{\text{CS}}(\cdot, \cdot)$ ensures that the selected description set contains as little repetitive or redundant textual content as possible. The use of $f_{\text{TopK}}(\cdot, \cdot)$ minimizes the presence of distracting descriptions in the candidate description set (e.g., noisy text generated by an LLM). When $f_{\text{CoS}}(T_i, D) = 0$, the description set D remains unchanged. However, if $f_{\text{CoS}}(T_i, D) = 1$, D will be appended with the new description T_i, i.e., $D \leftarrow D \cup \{T_i\}$.

Overall, by applying these functions, the descriptions becomes more diverse under fixed set size $|D|$, effectively increasing the number of useful descriptions. This is equivalent to performing *description refinement*.

[1] https://en.wikipedia.org/wiki/Jaccard_index

4.3 Overall Pipeline

The overall pipeline of BiFTA is illustrated in Figure 3. From the Image Flow illustrated in the figure, BiFTA performs View Refinement to the randomly cropped image patches. Each patch is stored in a fixed size queue V, while each image patch is filtered using the IoU filter f_{IoU}, as defined in Eq. 2. From the Text Flow illustrated on the other side of the figure, BiFTA conducts Description Refinement on a set of textual descriptions. The candidate texts are first filtered by the CoS filter f_{CoS} and then ranked according to their top-k similarity scores with the label prompt. Finally, the similarity between the refined views and descriptions is computed using Eq. 1 to yield the final prediction. The detailed algorithm is provided in Appendix A.

4.4 Understanding BiFTA Through Posterior Probability

In this section, we will explain that the label predictions obtained using our method contain more effective views and descriptions through the angle of posterior probability.

We will first define the concept of *Redundant Views/Descriptions* in Definition 1 and *Deduplicated Set* in Definition 2.

Definition 1. *(Redundant Views/Descriptions). Assuming I_i and I_j are two views of image x, if $\text{IoU}(I_i, I_j) \geq 1-\delta$, where $1-\delta$ is the IoU threshold, then I_i and I_j are considered to have a significant overlap, i.e., I_i and I_j are redundant views of each other. Regarding textual descriptions T_p and T_q for label y, if $\cos(f_{\text{txt}}(T_p), f_{\text{txt}}(T_q)) \geq 1-\epsilon$, where $1-\epsilon$ is the threshold, then the two descriptions can be considered nearly identical, i.e., they are mutually redundant descriptions.*

Definition 2. *(BiFTA-Deduplicated Set). For a set containing views $V = \{I_1, I_2, ..., I_n\}$ with the size n, V is a deduplicated view set if and only if it satisfies:*

$$\forall I_i, I_j \in V, \text{IoU}(I_i, I_j) < 1-\delta.$$

Similarly, for a set $D = \{T_1, T_2, ..., T_m\}$ containing m descriptions, D is a deduplicated description set if and only if it satisfies:

$$\forall T_p, T_q \in D, \cos(f_{\text{txt}}(T_p), f_{\text{txt}}(T_q)) < 1-\epsilon.$$

Through Definition 2 and Section 4.1 to 4.3, it can be concluded that view and description sets used by our method are BiFTA-deduplicated set. However, view and description sets utilized in WCA do not belong to BiFTA-deduplicated sets, as no constraints are established during random cropping of images or sampling of description texts.

Proposition 3. *For a pair of redundant views I_i and I_j (cf. Definition 1), when $\delta \to 0$, then for a label y, it can be obtained that $p(I_i|y) \approx p(I_i, I_j|y)$. Similarly, for a pair of redundant descriptions T_p and T_q, assuming the text encoder $f_{\text{txt}}(\cdot)$ is an injective function, when $\epsilon \to 0$, then $p(T_p|y) \approx p(T_p, T_q|y)$.*

Proposition 3 states that as δ approaches 0, the conditional probability of two mutually redundant views given the label y approximately equals the conditional probability of one of the views given y. The redundancy descriptions follow accordingly. See detailed proof of Proposition 3 in Appendix B.1.

Proposition 4. *Assuming that the label $y \in \mathcal{Y}$ follows a uniform distribution, then applying our method, the posterior probability of y can be formulated as:*

$$\hat{p}_{\text{ours}}(y|I_1, I_2, ..., I_n, T_1, T_2, ..., T_m) \propto p(I_1, I_2, ..., I_n, T_1, T_2, ..., T_m|y),$$

where both $\{I_1, I_2, ..., I_n\}$ and $\{T_1, T_2, ..., T_m\}$ are BiFTA-deduplicated sets (cf.Definition 2). Under the same condition in Proposition 3, when applying WCA, the posterior probability can be estimated as:

$$\hat{p}_{\text{wca}}(y|I'_1, I'_2, ..., I'_n, T'_1, T'_2, ..., T'_m) \propto p(V', D'|y),$$

where V' and D' are the largest dedupicated set satisfying $V' \subseteq \{I'_1, I'_2, ..., I'_n\}, D' \subseteq \{T'_1, T'_2, ..., T'_m\}$. The actual effective numbers of views and descriptions should be less than or equal to that of our method (i.e., $|V'| \leq m, |D'| \leq n$).

According to Proposition 4 (proved in Appendix B.2), when the numbers of views and descriptions are fixed, our refinement-and-filtering approach prioritizes the more effective ones while filtering out redundant information. This is equivalent to increasing the number of effective views and descriptions after removing duplicated ones.

5 Experiment

First, we outline the complete experimental settings in Section 5.1. In summary, we evaluate the refinement performance of BiFTA through extensive experiments on 6 benchmark datasets and 5 different backbone architectures of the CLIP model. To further demonstrate the generalizability of our framework, we additionally conduct experiments on other VLM architectures in Appendix C, including ALIGN (Jia et al., 2021), AltLIP (Chen et al., 2022), GroupViT (Xu et al., 2022), and SigLIP (Zhai et al., 2023), which suggest that BiFTA consistently improves cross-alignment methods. In Section 5.2, we primarily present the zero-shot classification performance of the CLIP model with a ViT-B/32 backbone across 6 downstream tasks. The rest experimental results for other CLIP backbones are provided in Tables 8-10 in Appendix C. In Section 5.3, we conduct ablation studies to validate the design principles of *view refinement* and *description refinement*. For completeness, we further explore alternative refinement strategies in Appendix **??**. Finally, the limitations of our work are discussed in Appendix F.

5.1 Experimental Settings

Datasets. To evaluate BiFTA, we conduct experiments on 6 downstream classification tasks under a zero-shot setting, including: (1) ImageNet (Deng et al., 2009), a large-scale dataset comprising 1,000 diverse object classes; (2) CUB (Welinder et al., 2010), a fine-grained dataset of 200 bird species, focusing on subtle visual distinctions; (3) Oxford Pets (Parkhi et al., 2012), a dataset of 37 pet categories; (4) DTD (Cimpoi et al., 2014), a texture dataset containing 47 categories of materials and surfaces; (5) Food101 (Bossard et al., 2014), a dataset of 101 food categories; and (6) Place365 (Zhou et al., 2017), a scene recognition dataset with 365 categories of indoor and outdoor environments. These datasets span a wide range of categories, which encompass various visual domains such as scenes, textures, food, animals and fine-grained objects. Thus, the evaluation ensures the robustness and generalizability of BiFTA across various real-world applications.

Baselines. We evaluate the performance of BiFTA by comparing it with 6 competitive baselines on zero-shot classification: (1) CLIP (Radford et al., 2021), a naive approach that incorporates a manually crafted label prompt; (2) Ensemble CLIP (CLIP-E) (Radford et al., 2021), an advance approach that incorporates a series of label prompts; (3) CLIP-D (Menon & Vondrick, 2023), an approach that utilizes category descriptions generated by a LLM instead of label prompting approach; (4) Waffle (Roth et al., 2023), a novel approach that replaces LLM-generated category descriptions with random word descriptions; (5) CuPL (Pratt et al., 2023), a method that leverages LLM and improves the quality and variety of textual descriptions compared with CLIP-D; (6) WCA (Li et al., 2024), a recently proposed method that computes cross-alignment scores between localized image patches and fine-grained textual descriptions.

Implementation Details. We primarily use the pre-trained CLIP model for main experiments, including both *Vision Transformer* (ViT) and ResNet backbone architectures, specifically ViT-B/32, ViT-B/16, ViT-L/14, RN-50 and RN-101. These architectures are selected to enable a thorough analysis of the proposed method across varying scales and complexities. We keep the shared hyperparameters consistent with the settings in WCA (Li et al., 2024): we use $n = 60$ for the patch queue length $|V|$ and $m = 50$ for the number of textual descriptions per category. We keep the cropping window size consistent with WCA, ranging from $[\alpha_{\textbf{low}}, \beta_{\textbf{high}}]$, where $\alpha_{\textbf{low}} = 0.5$ and $\beta_{\textbf{high}} = 0.9$ across all experiments. Additionally, we store the embeddings of localized image patches during the initial execution (Li et al., 2024), which allows them to be reused when evaluating different sets of textual descriptions, thereby significantly reducing computational costs.

5.2 Zero-shot Classification Results

Tables 1 to 2 present the zero-shot classification results across six downstream tasks, with each table corresponding to a different CLIP backbone architecture.

Table 1: Zero-shot classification accuracy (%) across various baseline methods with the pre-trained CLIP model (ViT-B/32). We report the averaged results and standard deviations σ of 20 runs, with the improvement Δ(%) over the top-performing baseline WCA highlighted in **green**. The results of our method are highlighted and we use **bold** to represent the best-performing method.

Method	ImageNet	CUB	Oxford Pets	DTD	Food101	Place365
CLIP	62.05	51.21	85.04	42.93	82.60	38.51
CLIP-E	63.37	52.74	87.38	43.83	83.93	39.28
CLIP-D	63.01	52.69	84.46	44.20	84.12	39.90
Waffle	63.30	52.04	85.50	42.98	83.98	39.47
CuPL	64.37	49.76	87.03	47.50	84.20	39.08
WCA	66.49	56.74	89.05	49.89	86.11	40.55
BiFTA (ours)	**66.58±0.06**	**58.24±0.17**	**89.74±0.14**	**53.22±0.26**	**86.43±0.06**	**41.55±0.06**
Δ	**+0.09**	**+1.50**	**+0.69**	**+3.33**	**+0.32**	**+1.00**

Table 2: Zero-shot classification accuracy (%) across various baseline methods with the pre-trained CLIP model (ViT-L/14). We report the averaged results and standard deviations σ of 20 runs, with the improvement Δ(%) over the top-performing baseline WCA highlighted in **green**. The results of our method are highlighted and we use **bold** to represent the best-performing method.

Method	ImageNet	CUB	Oxford Pets	DTD	Food101	Place365
CLIP	73.48	62.12	93.24	52.61	92.55	39.63
CLIP-E	75.52	62.53	93.62	55.43	93.07	40.55
CLIP-D	75.03	63.26	93.30	55.05	93.03	40.55
Waffle	75.31	62.27	91.55	54.31	93.33	40.89
CuPL	76.62	62.15	94.33	60.59	93.37	40.77
WCA	77.32	65.12	94.67	61.74	93.93	42.19
BiFTA (ours)	**77.82±0.04**	**65.67±0.13**	**94.96±0.10**	**62.45±0.26**	**93.97±0.04**	**42.98±0.05**
Δ	**+0.50**	**+0.55**	**+0.29**	**+0.71**	**+0.04**	**+0.79**

Table 3: Average classification accuracy (%) across various baseline methods with different CLIP models. The improvements Δ(%) over the top-performing baseline (i.e., WCA) are highlighted in **green**. We use **bold** to represent the best-performing method and underlined to represent the second-best method.

Model Architecture	CLIP	CLIP-E	CLIP-D	Waffle	CuPL	WCA	BiFTA (ours)	Δ
ViT-B/32	60.39	61.76	61.40	61.21	62.16	64.81	**65.96**	**+1.15**
ViT-B/16	63.59	64.51	64.67	64.34	66.09	67.87	**68.29**	**+0.42**
ViT-L/14	68.94	70.12	69.87	69.61	71.31	72.50	**72.98**	**+0.48**
RN-50	56.97	58.64	58.39	57.92	60.01	62.00	**62.54**	**+0.54**
RN-101	59.14	60.50	59.22	58.89	59.04	61.14	**62.03**	**+0.89**

In Table 1, the classification performance of CLIP (B/32) underscores the consistent superiority of BiFTA over all baselines. In specific, BiFTA achieves an average performance gain of Δ_{avg} = **1.15**% compared to WCA across all downstream tasks and outperforms previous baselines that only utilize label prompts by a large margin. Notably, BiFTA achieves a **3.33**% improvement in accuracy over the WCA scoring method on the DTD dataset, which consists of diverse texture patterns. This improvement stems from the inherent challenge of the dataset: textual patterns in DTD are often homogeneous, where random cropping strategy tends to produce semantically similar regions. In BiFTA, *view refinement* systematically eliminates redundant image patches through the IoU filter function. The image patch queue V is thereby maintained as a de-duplicated set consisting of semantically independent candidates. In Eq. 1, each selected image patch is

Table 4: Comparison of Top-1 accuracy (%) across alternative VLM architectures under zero-shot classification setting. All models are evaluated on the ImageNet-1K benchmark.

VLMs	`Vanilla`	`Vanilla_E`	`Vanilla_D`	`Waffle`	`CuPL`	`WCA`	`BiFTA`
ALIGN	65.24	65.79	65.08	65.22	66.24	66.61	**67.15**
AltLIP	73.79	74.86	74.48	74.29	75.74	76.20	**76.88**
GroupViT	37.11	42.72	40.10	40.42	44.53	45.27	**45.31**
SigLIP	76.18	76.22	76.51	76.10	77.04	77.40	**77.74**

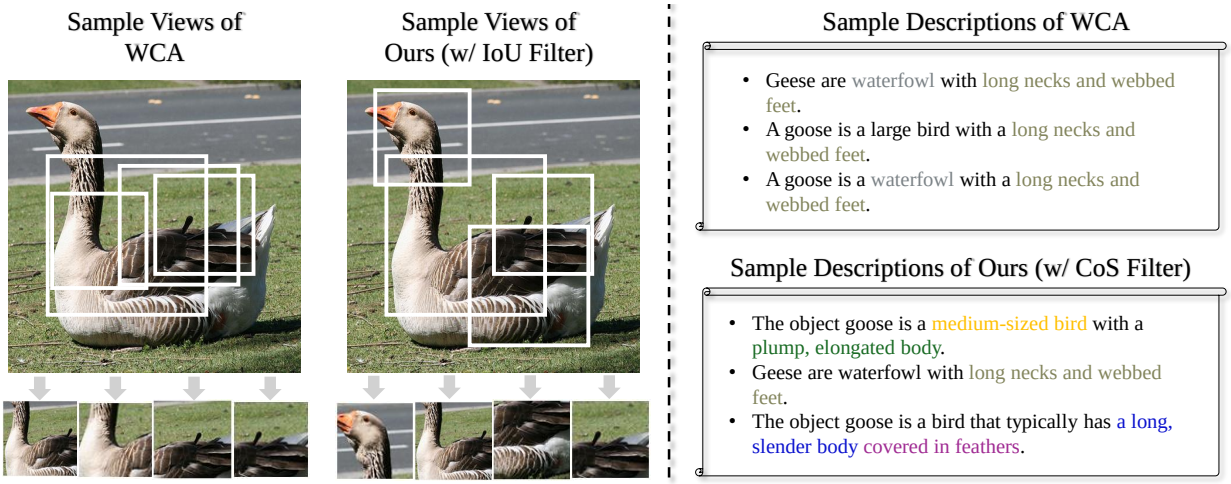

Figure 4: A visualization comparing the effectiveness of *view refinement* and *description refinement* in BiFTA against WCA. **Left**: with an IoU filter, the cropped samples exhibit diverse and distinctive localized features. **Right**: with a CoS filter, the texts can describe various local features of a category.

assigned a corresponding visual weight w_i. This weight factor ensures that discriminative visual features dominate the computation of the cross-alignment score, thereby enhancing the model's robustness against repetitive patterns such as the textures in DTD dataset. The text weight factor v_j follows analogously, where it highlights semantically distinctive textual descriptions. In Table 2, we observe that BiFTA consistently outperforms all baseline methods when evaluated with a large-scale backbone (ViT-L/14). Notably, it achieves a (+0.50%) improvement on ImageNet, which is a significant gain for such a high-capacity model. Furthermore, in Table 3, BiFTA exhibit similar trend observed in WCA that smaller backbone models (e.g., B/32) exhibit more significant improvements (+1.15%) comparing with their larger counterparts (e.g., L/14), (+0.48%). This consistency confirms that our refinements retain the visual-text cross-alignment principles of WCA. The experimental results obtained with the other CLIP backbones and alternative VLM architectures are reported in Appendix C. In Table 3, we summarize the average performance of each CLIP backbone across the evaluated benchmarks. The results clearly demonstrate that BiFTA consistently outperforms all baseline methods across all CLIP backbone models. In specific, BiFTA achieves an average accuracy improvement of 0.42% to 0.90% across thoses benchmarks compared to the WCA scoring method.

In Table 4, we report a supplementary experiment that evaluates the performance of BiFTA under alternative VLM architectures. This consistency underscores the adaptability and effectiveness of our refinement method when applied to a diverse range of VLMs. For ease of distinguishing VLM names from method names, we denote CLIP and its two variants (CLIP-E and CLIP-D) as `Vanilla`, `Vanilla_E`, and `Vanilla_D` in Table 4.

For a clearer visual comparison, Figure 4 illustrates the differences between BiFTA and WCA. On the left, given an image of a goose, BiFTA successfully filters out semantically independent regions (e.g., head, wings,

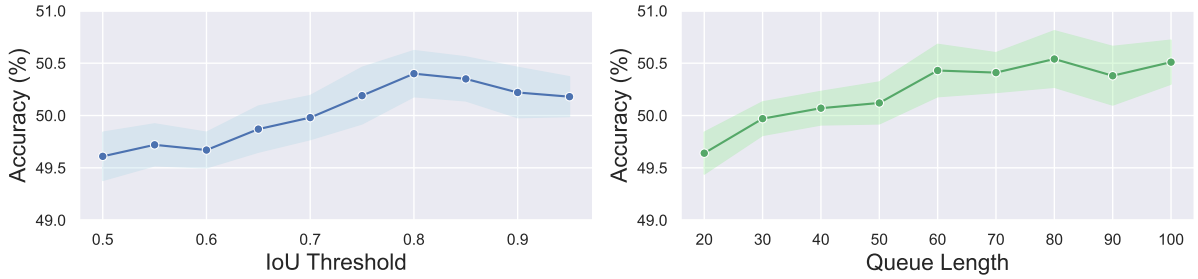

Figure 5: **Left**: Accuracy of using alternative IoU thresholds on DTD dataset with CLIP (B/32). **Right**: Accuracy of changing the size of $|V|$ on DTD dataset with CLIP (B/32).

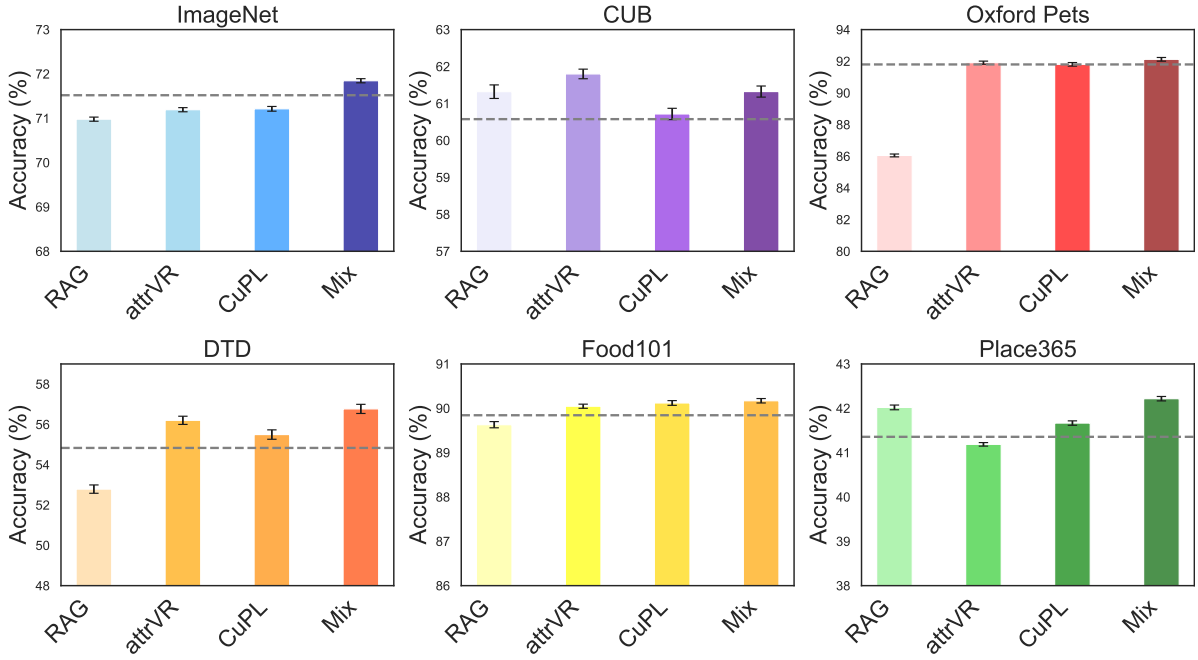

Figure 6: Comparing *view refinement* with different description sets and strategies on BiFTA. The results are averaged across 3 image encoder backbones of the CLIP model, where 'mix' is the strategy BiFTA finally utilized for *view refinement*.

neck, and fur), whereas WCA usually produces overlapping image patches (e.g., repeated neck regions or background noise) so that ignores valuable features. This highlights how *view refinement* mitigates feature redundancy through IoU-guided filtering. On the right, text samples describing a goose are presented. Descriptions refined by the CoS Filter are notably more diverse and distinctive: semantically meaningful prompts such as "plump, elongated body" and "a long, slender body" are preserved, while redundant phrases like "long necks and webbed feet" are pruned. This demonstrates the effectiveness of *description refinement* in promoting semantic diversity among textual inputs.

5.3 Hyperparameter Analysis and Ablation Studies

Hyperparameter tuning. Figure 5 illustrates the impact of varying hyperparameter values on downstream performance: IoU threshold $\eta = 1 - \delta$ and patch queue length $N = |V|$. On the left, the classification accuracy varies as the η changes, with accuracy gradually rising and then dropping as η increases, which suggest that a moderate η is needed to achieve an optimal performance. In practice, a lower η will result in a critic cut-off to the cropped image patches, which often results in the de-duplicated queue V containing an

Table 5: Ablation studies of comparing the performance of WCA and BiFTA between single modality refinement (w/o VR and w/o DR) and full refinements, using CLIP models (B/32, B/16 and L/14). **VR**: View Refinement; **DR**: Description Refinement. The best result for a single dataset across each model is underlined, and the best averaged results (%) are highlighted in **bold**.

	Methods	ImageNet	CUB	Oxford Pets	DTD	Food101	Place365	Avg.
B/32	WCA	66.49	56.74	89.05	49.89	86.11	40.55	64.81
	BiFTA (w/o VR)	66.51	58.11	88.56	51.27	86.41	41.80	65.44
	BiFTA (w/o DR)	66.77	56.94	89.17	50.51	87.46	40.85	65.28
	BiFTA (ours)	66.58	58.24	89.74	53.22	86.43	41.55	**65.96**
B/16	WCA	71.05	59.87	92.13	52.87	89.99	41.33	67.87
	BiFTA (w/o VR)	70.67	59.36	90.58	51.36	90.20	42.23	67.40
	BiFTA (w/o DR)	71.10	59.91	91.83	53.56	90.38	42.11	68.15
	BiFTA (ours)	71.14	60.06	91.67	54.64	90.11	42.12	**68.29**
L/14	WCA	77.32	65.12	94.67	61.74	93.93	42.19	72.50
	BiFTA (w/o VR)	77.14	65.46	94.63	62.09	93.94	42.51	72.63
	BiFTA (w/o DR)	77.89	65.56	94.78	62.17	94.04	42.58	72.84
	BiFTA (ours)	77.82	65.67	94.96	62.45	93.97	42.98	**72.98**

insufficient number of samples. To simply address this limitation, we re-sample from the existing queue until N samples are obtained. However, this procedure inevitably introduces redundant patches into V, thereby violating the principle of maintaining a de-duplicated set. As shown in the left panel of Figure 5, this trend further indicates that redundant information can adversely affect downstream task performance. Notably, *view refinement* becomes ineffective as η approaches 1 due to the overly loose restriction on the cut-off. The performance exhibits a decreasing trend once IoU exceeds 0.80, which is expected since the views are no longer effectively constrained by our *view refinement*. The right panel of Figure 5 shows that increasing the queue length N has a consistently positive impact on classification accuracy, whereas the increasing trend reaches a plateau at $N = 60$. For consistency, we set $\eta = 0.80$ and $N = 60$ across all experiments.

Ablation studies of alternative description refinement. Figure 6 presents the ablation results of using different sets of textual descriptions. These descriptions are generated by LLMs with various prompt template designs, as introduced in Section 4.2. Among all settings, only the mixed description set from our *description refinement* demonstrates consistently superior performance across most downstream tasks, with results averaged over three CLIP backbones: ViT-B/32, ViT-B/16, and ViT-L/14. The dashed line indicates the average performance of WCA, which is the strongest baseline method. Relatively, BiFTA achieves varying degrees of improvement depending on the description set. Notably, descriptions generated with RAG-prompt templates perform unsatisfactorily compared with other sets, and details of their implementation are provided in Appendix D. In addition, CuPL is equivalent to applying only the *view refinement* component of BiFTA, we also provide quantitative result in Table 5. This suggests that even refining a single modality (the visual side) is sufficient to improve zero-shot image classification performance.

Ablation studies of BiFTA w/o view refinement and description refinement. We also compare the experimental results of the WCA scoring method with a complete version of BiFTA and partial BiFTA in Table 5. We demonstrate that applying BiFTA refinement to a single modality is sufficient to improve cross-alignment performance. For ImageNet and Food101 datasets, the models often exhibit better performance with BiFTA w/o description refinements, which indicates our merged description set might not be an optimal description set. Overall, BiFTA with dual refinements achieves the highest average improvement across all three CLIP backbones, as shown in Table 5.

$$f_{\text{CLIP}}(I_i, V) = \begin{cases} 1 & \forall I \in V, \cos(f_{\text{img}}(I), f_{\text{img}}(I_i)) < 1 - \epsilon \\ 0 & \exists I \in V, \cos(f_{\text{img}}(I), f_{\text{img}}(I_i)) \geq 1 - \epsilon \end{cases},$$

Table 6: Performance comparison among two alternative *View Refinement* (VR) strategies.

VR	ImageNet	CUB	Oxford Pets	DTD	Food101	Place365	Avg.
f_{IoU}	66.77	56.94	89.17	50.51	87.46	40.85	65.28
f_{CLIP}	66.93	55.41	88.48	52.10	88.21	40.94	**65.35**

Table 7: Performance comparison among two alternative *Description Refinement* (DR) strategies.

DR	ImageNet	CUB	Oxford Pets	DTD	Food101	Place365	Avg.
$f_{\text{TF-IDF}}$	66.38	58.05	88.74	51.25	86.19	42.14	**65.46**
f_{CS}	66.51	58.11	88.56	51.27	86.41	41.80	65.44

$$f_{\text{TF-IDF}}(T_i, D) = \begin{cases} 1 & \forall T \in D, \cos(f_{\text{emb}}(T), f_{\text{emb}}(T_i)) < 1 - \epsilon \\ 0 & \exists T \in D, \cos(f_{\text{emb}}(T), f_{\text{emb}}(T_i)) \geq 1 - \epsilon \end{cases},$$

Exploring Alternative Refinement Strategies. Table 6 - 7 illustrate the result of the downstream tasks by utilizing alternative View/Description Refinement strategies. For alternative *view refinement* strategies, we attempt to directly use the image encoder of the CLIP model f_{img} to obtain the embeddings of each image patch. Then we incorporate cosine similarity to select the redundant views, as shown in Eq. 3. As a result, f_{CLIP} offers slight improvements in zero-shot classification on downstream tasks. However, computing image patch embeddings is highly computationally intensive, since each sample must be divided into N patches. To make our framework practical, data refinement procedure should be designed in a lightweight manner that minimizes additional computational overhead. In contrast, f_{IoU} achieves a favorable balance between efficiency and performance.

For alternative *description refinement* strategies, we leverage TF-IDF to encode the text descriptions into text embeddings (Jones, 2004), denoted as f_{emb}. Then, we incorporate f_{emb} into a compositional function $f_{\text{TF-IDF}}$ to eliminate duplicate text descriptions, as shown in Eq. 3. Similar to the proposed f_{CoS} in Section 4.2, we obtain the final filtering function $f(T_i, D) = f_{\text{TF-IDF}}(T_i, D) \cdot f_{\text{TopK}}(T_i, D)$. The results indicate that the two description refinement strategies yield nearly identical performance. Nevertheless, both consistently outperform the baselines. The core of DR lies in leveraging the f_{TopK} function to select the most semantically relevant descriptions to the label prompt after an initial filtering step with either f_{CS} or $f_{\text{TF-IDF}}$. Overall, lightweight yet principled refinement strategies are sufficient to yield competitive gains without incurring excessive computational overhead.

6 Conclusion

In this work, we identified a critical limitation in existing fine-grained visual-text alignment methods: the presence of redundant information in both localized image patches and LLM-generated textual descriptions. To address this, we propose BiFTA, a novel framework that introduces two key innovations: (1) *view refinement* via IoU-based filtering to eliminate spatially overlapping image patches, and (2) *description refinement* through cosine similarity thresholding to remove semantically redundant textual descriptions. Our experiments across 6 benchmark datasets demonstrate that BiFTA consistently outperforms state-of-the-art methods in zero-shot classification accuracy over the previous methods. The ablation studies validate the necessity of both components: IoU filtering ensures diverse visual features, while cosine-based text pruning enhances semantic specificity. Theoretical analysis further justifies our method by linking redundancy reduction to improved posterior probability estimation in multi-modal alignment.

References

Jean-Baptiste Alayrac, Jeff Donahue, Pauline Luc, Antoine Miech, Iain Barr, Yana Hasson, Karel Lenc, Arthur Mensch, Katherine Millican, Malcolm Reynolds, Roman Ring, Eliza Rutherford, Serkan Cabi, Tengda Han, Zhitao Gong, Sina Samangooei, Marianne Monteiro, Jacob L. Menick, Sebastian Borgeaud, Andy Brock, Aida Nematzadeh, Sahand Sharifzadeh, Mikolaj Binkowski, Ricardo Barreira, Oriol Vinyals, Andrew Zisserman, and Karén Simonyan. Flamingo: a visual language model for few-shot learning. In *NeurIPS*, 2022.

Lukas Bossard, Matthieu Guillaumin, and Luc Van Gool. Food-101–mining discriminative components with random forests. In *ECCV*, 2014.

Tom B. Brown, Benjamin Mann, Nick Ryder, Melanie Subbiah, Jared Kaplan, Prafulla Dhariwal, Arvind Neelakantan, Pranav Shyam, Girish Sastry, Amanda Askell, Sandhini Agarwal, Ariel Herbert-Voss, Gretchen Krueger, Tom Henighan, Rewon Child, Aditya Ramesh, Daniel M. Ziegler, Jeffrey Wu, Clemens Winter, Christopher Hesse, Mark Chen, Eric Sigler, Mateusz Litwin, Scott Gray, Benjamin Chess, Jack Clark, Christopher Berner, Sam McCandlish, Alec Radford, Ilya Sutskever, and Dario Amodei. Language models are few-shot learners. In *NeurIPS*, 2020.

Chengyi Cai, Zesheng Ye, Lei Feng, Jianzhong Qi, and Feng Liu. Attribute-based visual reprogramming for image classification with CLIP. *arXiv preprint arXiv:2501.13982*, 2025.

Chi-Min Chan, Chunpu Xu, Ruibin Yuan, Hongyin Luo, Wei Xue, Yike Guo, and Jie Fu. RQ-RAG: learning to refine queries for retrieval augmented generation. *arXiv preprint arXiv:2404.00610*, 2024.

Zhongzhi Chen, Guang Liu, Bo-Wen Zhang, Fulong Ye, Qinghong Yang, and Ledell Wu. Altclip: Altering the language encoder in clip for extended language capabilities. In *ACL (Findings)*, 2022.

Jaemin Cho, Jie Lei, Hao Tan, and Mohit Bansal. Unifying vision-and-language tasks via text generation. In *ICML*, 2021.

Mircea Cimpoi, Subhransu Maji, Iasonas Kokkinos, Sammy Mohamed, and Andrea Vedaldi. Describing textures in the wild. In *CVPR*, 2014.

Fangming Cui, Yonggang Zhang, Xuan Wang, Xule Wang, and Liang Xiao. Generalizable prompt learning of clip: A brief overview. *arXiv preprint arXiv:2503.01263*, 2025.

Jia Deng, Wei Dong, Richard Socher, Li-Jia Li, Kai Li, and Li Fei-Fei. Imagenet: A large-scale hierarchical image database. In *CVPR*, 2009.

Jacob Devlin, Ming-Wei Chang, Kenton Lee, and Kristina Toutanova. BERT: pre-training of deep bidirectional transformers for language understanding. In *NAACL-HLT*, 2019.

Zirui Guo, Lianghao Xia, Yanhua Yu, Tu Ao, and Chao Huang. Lightrag: Simple and fast retrieval-augmented generation. *arXiv preprint arXiv:2410.05779*, 2024.

Xiangteng He and Yuxin Peng. Fine-grained image classification via combining vision and language. In *CVPR*, 2017.

Chao Jia, Yinfei Yang, Ye Xia, Yi-Ting Chen, Zarana Parekh, Hieu Pham, Quoc V. Le, Yun-Hsuan Sung, Zhen Li, and Tom Duerig. Scaling up visual and vision-language representation learning with noisy text supervision. In *ICML*, 2021.

Karen Spärck Jones. A statistical interpretation of term specificity and its application in retrieval. *J. Documentation*, 2004.

Wonjae Kim, Bokyung Son, and Ildoo Kim. Vilt: Vision-and-language transformer without convolution or region supervision. In *ICML*, 2021.

Jinhao Li, Haopeng Li, Sarah Monazam Erfani, Lei Feng, James Bailey, and Feng Liu. Visual-text cross alignment: Refining the similarity score in vision-language models. In *ICML*, 2024.

Junnan Li, Dongxu Li, Caiming Xiong, and Steven C. H. Hoi. BLIP: bootstrapping language-image pre-training for unified vision-language understanding and generation. In *ICML*, 2022a.

Wanhua Li, Xiaoke Huang, Zheng Zhu, Yansong Tang, Xiu Li, Jie Zhou, and Jiwen Lu. Ordinalclip: Learning rank prompts for language-guided ordinal regression. In *NeurIPS*, 2022b.

Xiang Lisa Li and Percy Liang. Prefix-tuning: Optimizing continuous prompts for generation. In *ACL*, 2021.

Weixin Liang, James Zou, and Zhou Yu. ALICE: active learning with contrastive natural language explanations. In *EMNLP*, 2020.

Sachit Menon and Carl Vondrick. Visual classification via description from large language models. In *ICLR*, 2023.

Omkar M Parkhi, Andrea Vedaldi, Andrew Zisserman, and CV Jawahar. Cats and dogs. In *CVPR*, 2012.

Sarah M. Pratt, Ian Covert, Rosanne Liu, and Ali Farhadi. What does a platypus look like? generating customized prompts for zero-shot image classification. In *ICCV*, 2023.

Alec Radford, Karthik Narasimhan, Tim Salimans, Ilya Sutskever, et al. Improving language understanding by generative pre-training. OpenAI, 2018.

Alec Radford, Jeffrey Wu, Rewon Child, David Luan, Dario Amodei, Ilya Sutskever, et al. Language models are unsupervised multitask learners. *OpenAI blog*, 2019.

Alec Radford, Jong Wook Kim, Chris Hallacy, Aditya Ramesh, Gabriel Goh, Sandhini Agarwal, Girish Sastry, Amanda Askell, Pamela Mishkin, Jack Clark, Gretchen Krueger, and Ilya Sutskever. Learning transferable visual models from natural language supervision. In *ICML*, 2021.

Karsten Roth, Jae Myung Kim, A Koepke, Oriol Vinyals, Cordelia Schmid, and Zeynep Akata. Waffling around for performance: Visual classification with random words and broad concepts. In *ICCV*, 2023.

Manli Shu, Weili Nie, De-An Huang, Zhiding Yu, Tom Goldstein, Anima Anandkumar, and Chaowei Xiao. Test-time prompt tuning for zero-shot generalization in vision-language models. In *NeurIPS*, 2022.

Amanpreet Singh, Ronghang Hu, Vedanuj Goswami, Guillaume Couairon, Wojciech Galuba, Marcus Rohrbach, and Douwe Kiela. FLAVA: A foundational language and vision alignment model. In *CVPR*, 2022.

Korawat Tanwisuth, Shujian Zhang, Huangjie Zheng, Pengcheng He, and Mingyuan Zhou. Pouf: Prompt-oriented unsupervised fine-tuning for large pre-trained models. In *ICML*, 2023.

Feng Wang, Manling Li, Xudong Lin, Hairong Lv, Alex Schwing, and Heng Ji. Learning to decompose visual features with latent textual prompts. In *ICLR*, 2022.

Zirui Wang, Jiahui Yu, Adams Wei Yu, Zihang Dai, Yulia Tsvetkov, and Yuan Cao. Simvlm: Simple visual language model pretraining with weak supervision. In *ICLR*, 2021.

P. Welinder, S. Branson, T. Mita, C. Wah, F. Schroff, S. Belongie, and P. Perona. Caltech-UCSD Birds 200. Technical Report CNS-TR-2010-001, California Institute of Technology, 2010.

Chengyue Wu, Teng Wang, Yixiao Ge, Zeyu Lu, Ruisong Zhou, Ying Shan, and Ping Luo. π-tuning: Transferring multimodal foundation models with optimal multi-task interpolation. In *ICML*, 2023.

Jiarui Xu, Shalini De Mello, Sifei Liu, Wonmin Byeon, Thomas Breuel, Jan Kautz, and Xiaolong Wang. Groupvit: Semantic segmentation emerges from text supervision. In *CVPR*, 2022.

Hongwei Xue, Yupan Huang, Bei Liu, Houwen Peng, Jianlong Fu, Houqiang Li, and Jiebo Luo. Probing inter-modality: Visual parsing with self-attention for vision-and-language pre-training. In *NeurIPS*, 2021.

Jiahui Yu, Zirui Wang, Vijay Vasudevan, Legg Yeung, Mojtaba Seyedhosseini, and Yonghui Wu. Coca: Contrastive captioners are image-text foundation models. *TMLR*, 2022.

Yue Yu, Wei Ping, Zihan Liu, Boxin Wang, Jiaxuan You, Chao Zhang, Mohammad Shoeybi, and Bryan Catanzaro. Rankrag: Unifying context ranking with retrieval-augmented generation in llms. In *NeurIPS*, 2024.

Lu Yuan, Dongdong Chen, Yi-Ling Chen, Noel Codella, Xiyang Dai, Jianfeng Gao, Houdong Hu, Xuedong Huang, Boxin Li, Chunyuan Li, Ce Liu, Mengchen Liu, Zicheng Liu, Yumao Lu, Yu Shi, Lijuan Wang, Jianfeng Wang, Bin Xiao, Zhen Xiao, Jianwei Yang, Michael Zeng, Luowei Zhou, and Pengchuan Zhang. Florence: A new foundation model for computer vision. *arXiv preprint arXiv:2111.11432*, 2021.

Xiaohua Zhai, Basil Mustafa, Alexander Kolesnikov, and Lucas Beyer. Sigmoid loss for language image pre-training. In *ICCV*, 2023.

Bolei Zhou, Agata Lapedriza, Aditya Khosla, Aude Oliva, and Antonio Torralba. Places: A 10 million image database for scene recognition. *IEEE PAMI*, 2017.

Kaiyang Zhou, Jingkang Yang, Chen Change Loy, and Ziwei Liu. Learning to prompt for vision-language models. *IJCV*, 2022.

A Appendix 1: Additional Algorithms for the BiFTA Implementation

Algorithm 1 Zero-Shot Classification Pipeline of BiFTA

1: **Input** Query image $I_0 \in \mathbb{R}^{H \times W \times 3}$; labels $y \in \mathcal{Y}$; hyperparameters: a patch queue Q, crop count N, textual description count M, a label prompt $\hat{T}_y$, and pre-trained CLIP model with encoders $f_{\text{img}}(\cdot)$ (image) and $f_{\text{txt}}(\cdot)$ (text).
2: **Initialize** $Q \leftarrow [I_1]$ by Eq. 2
Step 1: View Refinement
3: **for** $i = 2$ to N **do**
4: **Generate** I_i by Eq. 2
5: **Check Is_Redundant**(I_i) by Algo. 2
6: **Is_Redundant**(I_i) == **false**, Q.push(I_i)
7: **Compute** $w_i = \text{softmax}(\cos(f_{\text{img}}(I_0), f_{\text{img}}(I_i)))$
8: **end for**
Step 2: Description Refinement
9: **for** $y \in \mathcal{Y}$ **do**
10: **Obtain** $\mathcal{T}^y = \{T_j\}_{j=1}^{J}$ where $J > M$
11: **Remove** $T_j \in \mathcal{T}^y$ based on Algo. 3
12: **Obtain** $\tilde{\mathcal{T}}^y \subseteq \mathcal{T}^y$ from Line (11)
13: **Initialize** $\hat{T}_y$
14: **Select top-**M Ts by $\arg\max_{T \in \tilde{\mathcal{T}}^y} \cos(f_{\text{txt}}(T), f_{\text{txt}}(\hat{T}_y))$
15: **Compute** v_j for all $\{T_j\}_{j=1}^{M}$ via $v_j = \text{softmax}(\cos(f_{\text{txt}}(\hat{T}_y), f_{\text{txt}}(T_j))$
16: **Compute** $\text{sim}^y_{\text{WCA}}$ via Eq. 1
17: **end for**
18: **Output** $y^* = \arg\max_{y \in \mathcal{Y}} \text{sim}^y_{\text{WCA}}$

Algorithm 2 Implementation of Redundant Image Patch Filtering

1: **Input:** A patch queue Q contains all the previous saved image patches, a new cropped image patch I_i, an IoU threshold $\eta = 1 - \delta$.
2: **Initialize Is_Redundant** == **false**
3: **for** $k = 1$ to $|Q|$ **do**
4: **Compute** $\eta_k = \text{IoU}(I_i, Q[k])$
5: **if** $\eta_k \geq \eta$ **then**
6: **Is_Redundant** $\leftarrow$ **true**, **break**
7: **end if**
8: **end for**
9: **Output: Is_Redundant**

Algorithm 3 Implementation of Redundant Textual Description Filtering

1: **Input:** A set of textual descriptions of label y, $\mathcal{T}^y = \{T_j\}_{j=1}^{J}$, where J is the number of descriptions in the merged textual description set; $\tau = 1 - \epsilon$ is the tolerance for the duplicate texts, setting to 1.0, f_{txt} is a text encoder.
2: **for** $j = 1$ to $J - 1$ **do**
3: **for** $k = j + 1$ to J **do**
4: **Compute** $S = \cos(f_{\text{txt}}(T_j), f_{\text{txt}}(T_k))$
5: **if** $S \geq \tau$ **then**
6: **Remove** T_k from $\mathcal{T}^y$
7: **end if**
8: **end for**
9: **end for**
10: **Obtain** $\tilde{\mathcal{T}}^y = \mathcal{T}^y$
11: **Output:** $\tilde{\mathcal{T}}^y$

B Appendix 2: Detailed Proof

B.1 Proof for Proposition 3

Proof.

Redundant Views: For views variables I_i and I_j, when $\delta \to 0$, we have $\text{IoU}(I_i, I_j) \to 1$.It means that two views are nearly completely overlapping, which is equivalent to:

$$||I_i - I_j||_2 \to 0,$$

where $||\cdot||_2$ represents the Euclidean norm.,

By applying the conditional probability formula, it is not difficult to obtain:

$$p(I_i|y) \cdot p(I_j|I_i, y) = p(I_i, I_j|y),$$

where:

$$p(I_j|I_i, y) = \frac{p(I_j, I_i, y)}{p(I_i, y)}.$$

As I_i nearly completely overlaps with I_j, we got: $p(I_i, y) \to p(I_j, I_i, y)$, and thus:

$$p(I_j|I_i, y) \to 1.$$

Conclusively, we have:

$$\lim_{\text{IoU}(I_i, I_j) \to 1} p(I_i|y) \to p(I_i, I_j|y).$$

Therefore, when $\delta \to 0$, we have $p(I_i|y) \approx p(I_i, I_j|y)$.

Redundant Descriptions: For description variable T_p and T_q, when $\epsilon \to 0$, we have $\cos(f_{\text{txt}}(T_p), f_{\text{txt}}(T_q)) \to 1$. It implies that the text embeddings of these two descriptions are nearly identical, which is equivalent to:

$$||f_{\text{txt}}(T_p) - f_{\text{txt}}(T_q)||_2 \to 0.$$

Similarly, following the same steps above, we will have:

$$\lim_{\cos(f_{\text{txt}}(T_p), f_{\text{txt}}(T_q)) \to 1} p(T_p|y) \to p(T_p, T_q|y).$$

Therefore, when $\epsilon \to 0$, assuming the fixed text encoder $f_{\text{txt}}(\cdot)$ is an injective function, we have $p(T_p|y) \approx p(T_p, T_q|y)$.

□

B.2 Proof for Proposition 4

According to Bayes' theorem, we can obtain

$$p(y|I_1, I_2, ..., T_n, T_1, T_2, ..., T_m) = \frac{p(I_1, I_2, ..., I_n, T_1, T_2, ..., T_m|y) \cdot p(y)}{p(I_1, I_2, ..., T_n, T_1, T_2, ..., T_m)}.$$

As is assumed, the downstream label $y \in \mathcal{Y}$ follows the uniform distribution. Therefore, the prior probability satisfies $p(y_i) = p(y_j), \forall y_i, y_j \in \mathcal{Y}$. Besides, $p(I_1, I_2, ..., T_n, T_1, T_2, ..., T_m)$ can be regarded as the normalization factor. Therefore, we have:

$$p(y|I_1, I_2, ..., T_n, T_1, T_2, ..., T_m) \propto p(I_1, I_2, ..., I_n, T_1, T_2, ..., T_m|y).$$

Applying V, D to represent the sets, we have $V = \{I_1, I_2, ..., I_n\}, D = \{T_1, T_2, ..., T_m\}$. We assume that $V' \in V, D' \in D$ represent the largest BiFTA-deduplicated sets of V, D. Then:

$$\forall I_i \in V - V' : \exists I_j \in V', \text{IoU}(I_i, I_j) \geq 1 - \delta, \text{and}$$

$$\forall I_i, I_j \in V, \text{IoU}(I_i, I_j) < 1 - \delta.$$

Similarly, for textual descriptions, we have:

$$\forall T_p \in D - D' : \exists T_q \in D', \cos(f_{\text{txt}}(I_i), f_{\text{txt}}(I_j)) \geq 1 - \epsilon, \text{and}$$

$$\forall T_p, T_q \in D, \cos(f_{\text{txt}}(I_i), f_{\text{txt}}(I_j)) < 1 - \epsilon.$$

For any I_i in $V - V'$, there exists an element $I_j \in V'$ such that I_i and I_j are mutually redundant. The same applies to the description set. Therefore, according to Proposition 3, we can obtain

$$p(y|I_1, I_2, ..., T_n, T_1, T_2, ..., T_m) \propto p(V, D|y) \approx p(V', D'|y).$$

Since the view sets and description sets obtained through our method are BiFTA-deduplicated sets, while the sets obtained by WCA are not BiFTA-deduplicated sets, the statement in Proposition 4 can be derived.

C Appendix 3: More Experimental Results

Table 8: Zero-shot classification accuracy (%) across various baseline methods with the pre-trained CLIP model (ViT-B/16). We report the averaged results and standard deviations σ of 20 runs, with the improvement Δ(%) over the top-performing baseline WCA highlighted in **green** and **red**. The results of our method are highlighted and we use **bold** to represent the best-performing method.

Method	ImageNet	CUB	Oxford Pets	DTD	Food101	Place365
CLIP	66.74	56.01	88.14	42.98	88.40	39.27
CLIP-E	68.37	56.16	89.10	45.27	88.83	40.30
CLIP-D	68.04	57.08	87.52	46.17	88.85	40.34
Waffle	68.12	56.89	86.51	44.68	89.06	40.76
CuPL	69.61	56.42	91.14	50.53	88.98	39.83
WCA	71.05	59.87	92.13	52.87	89.99	41.33
BiFTA (ours)	**71.14±0.04**	**60.06±0.15**	**91.67±0.11**	**54.64±0.16**	**90.11±0.05**	**42.12±0.04**
Δ	**+0.09**	**+0.19**	**-0.46**	**+1.77**	**+0.12**	**+0.79**

Table 9: Zero-shot classification accuracy (%) across various baseline methods with the ResNet-based CLIP model (RN-50). We report the averaged results and standard deviations σ of 20 runs, with the improvement Δ(%) over the top-performing baseline WCA highlighted in **green**. The results of our method are highlighted and we use **bold** to represent the best-performing method.

Method	ImageNet	CUB	Oxford Pets	DTD	Food101	Place365
CLIP	58.15	45.67	83.65	38.67	78.62	37.04
CLIP-E	59.82	46.58	85.66	41.22	80.82	37.73
CLIP-D	59.62	47.76	83.70	42.23	79.92	37.13
Waffle	59.82	46.76	83.54	38.88	80.74	37.77
CuPL	61.43	47.91	87.05	47.39	80.50	37.78
WCA	62.82	50.16	88.40	49.45	81.25	38.91
BiFTA (ours)	**63.54±0.06**	**50.43±0.17**	**88.74±0.12**	**51.41±0.22**	**81.39±0.09**	**39.70±0.06**
Δ	**+0.72**	**+0.27**	**+0.34**	**+1.96**	**+0.14**	**+0.79**

Tables 8 - 10 provide the results of utilizing alternative architectures of the CLIP backbone. The results show that BiFTA consistently outperforms baselines on downstream tasks with the ResNet-based backbone models, which evidently shows that our framework is able to generalize on various CLIP style models.

Table 10: Zero-shot classification accuracy (%) across various baseline methods with the ResNet-based CLIP model (RN-101). We report the averaged results and standard deviations σ of 20 runs, with the improvement Δ(%) over the top-performing baseline WCA highlighted in **green** and **red**. The results of our method are highlighted and we use **bold** to represent the best-performing method.

Method	ImageNet	CUB	Oxford Pets	DTD	Food101	Place365
CLIP	61.26	49.34	84.96	40.05	82.44	36.77
CLIP-E	62.31	49.65	86.97	43.62	83.64	37.81
CLIP-D	60.65	50.29	82.53	42.82	83.25	35.75
Waffle	61.25	48.05	83.70	40.05	82.48	37.83
CuPL	61.43	42.85	87.63	43.83	82.74	35.77
WCA	62.82	44.64	87.43	49.91	83.92	38.11
BiFTA (ours)	**65.24±0.05**	**45.86±0.12**	**86.81±0.15**	**50.87±0.23**	**84.02±0.05**	**39.40±0.06**
Δ	**+2.42**	**+1.22**	**-0.62**	**+0.96**	**+0.10**	**+1.29**

D Appendix 4: RAG-based Text Generation

We further investigate a novel prompt template based on *Retrieval-Augmented Generation (RAG)*, but the performance is unexpected as shown in figure 6. First, we begin by constructing a knowledge database using a pre-processed Wikipedia dataset [2] comprising 1.8 million documents. These document data are truncated, tokenized and encoded into embedding vectors using the "text-embedding-ada-002" text encoding model[3], which are then efficiently stored in the ChromaDB vector database. To generate textual descriptions, we manually craft a prompt template that integrates user queries with retrieved documents. The retrieval process relies on semantic similarity between the query and the database entries. These prompts are subsequently fed into a GPT model to produce the final textual descriptions. Despite these efforts, the resulting descriptions perform poorly when applied to CLIP-based classification tasks. Notably, we only utilize a small subset (approximately 150k documents) of the whole dataset, as it would take approximately 46 days to save those encoded documents into the database. Hence, we hypothesize that the retrieved documents may lack relevance to the target categories. Building on the RAG-prompt template, we consider that leveraging a larger database could further enhance the quality of textual descriptions. Accordingly, the description set may be improved by integrating RAG with a substantially larger database. We leave it as future work to explore whether expanding the database size could improve retrieval accuracy and then enhance the textual descriptions.

E Appendix 5: Extra Ablation Studies

Table 11: The ablation study on α. This experiment is evaluated on the ImageNet dataset by leveraging CLIP (B/32). We set the upper bound β to 0.9 and report the Top-1 Accuracy (%).

$\beta = 0.9$	α							
	0.1	0.2	0.3	0.4	0.5	0.6	0.7	0.8
WCA	66.48±0.07	66.57±0.07	66.61±0.06	66.72±0.07	66.49±0.07	66.85±0.04	66.92±0.04	66.93±0.05
Ours	66.93±0.06	66.97±0.05	67.05±0.08	67.24±0.04	66.58±0.06	66.88±0.04	66.61±0.04	66.55±0.07

Table 11 - 12 compare the Top-1 accuracy (%) of the WCA scoring method and BiFTA when varying the cropping size lower bound α and upper bound β. In Table 11, the results reveal a significant performance gap when the crop window range is large (e.g., $[0.1, 0.9]$). As α increases, image patches are cropped with larger window sizes, which reduces the effectiveness of the view filtering under stricter IoU thresholds. In Table 12, as β increases, there are more image patches with larger areas. We observe a consistent upward trend in

[2] https://huggingface.co/datasets/Salesforce/wikitext/viewer/wikitext-103-v1
[3] An embedding model published by OpenAI.

Table 12: The ablation study on β. This experiment is evaluated on the ImageNet dataset by leveraging CLIP (B/32). We set the lower bound α to 0.5 and report the Top-1 Accuracy (%).

$\alpha = 0.5$	β				
	0.6	0.7	0.8	0.9	1
WCA	61.77±0.06	63.21±0.05	64.45±0.05	66.49±0.07	66.06±0.08
Ours	64.40±0.07	65.46±0.07	65.91±0.05	66.58±0.06	66.73±0.08

accuracy as β increases for both methods. The performance gap gets more pronounced when β is smaller. For example, at $\beta = 0.6$, BiFTA achieves a 2.6% higher classification accuracy than WCA. This suggests that when the cropping windows are smaller, redundant small patches have a more significant negative impact on the weighted scores, whereas this issue is effectively addressed by integrating the *view refinement* introduced in BiFTA.

Based on Figure 6 in Section 5.3, we provide supplementary results for each backbone. Figures 7 to 9 present the classification accuracy across all downstream tasks for 4 description sets. Each sub-figure represents the results obtained from CLIP ViT-B/32, ViT-B/16 and ViT-L/14, respectively. In conclusion, the mixed set of descriptions, combining the CuPL and AttrVR descriptions and filtering them based on CoS function and top-k similarities, demonstrates superior performance compared to other description sets.

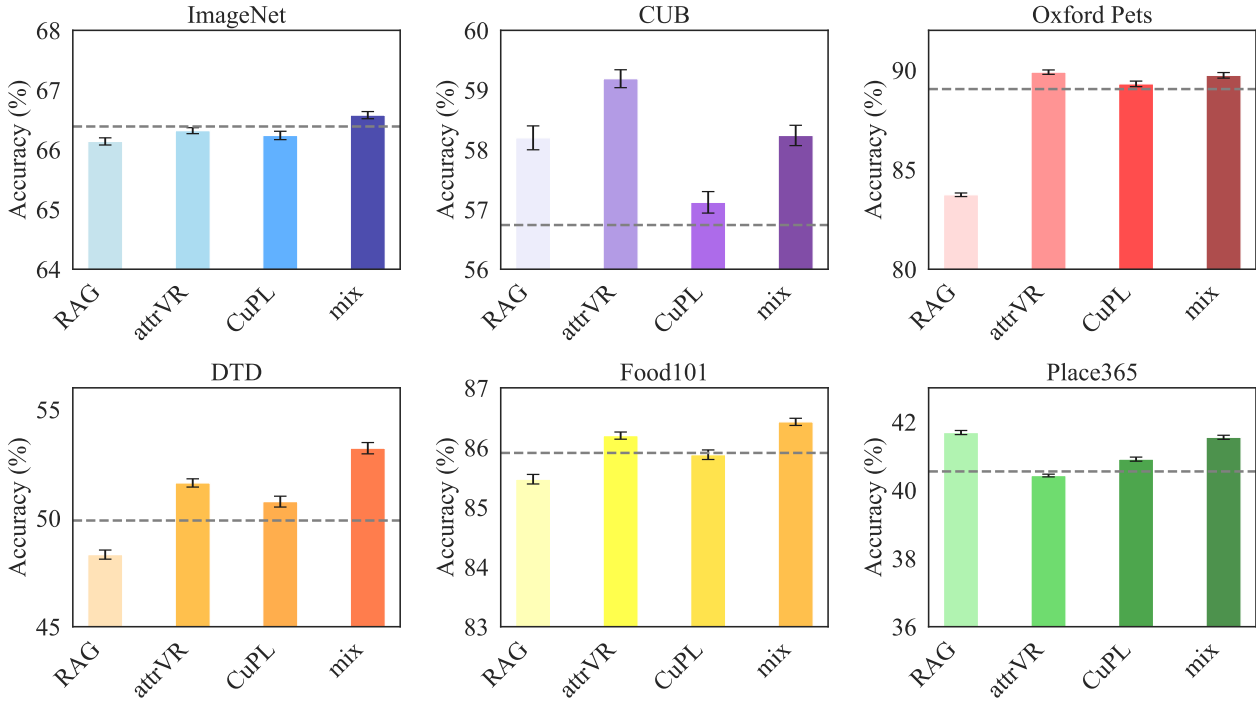

Figure 7: Results of exploring textual description studies, using the results of CLIP (B/32). “RAG” computes similarity using RAG-generated descriptions. “attrVR” uses both descriptive and distinctive texts to calculate similarity. “CuPL” directly employs descriptions from the CuPL method. “mix” combines “attrVR” and “CuPL” descriptions.

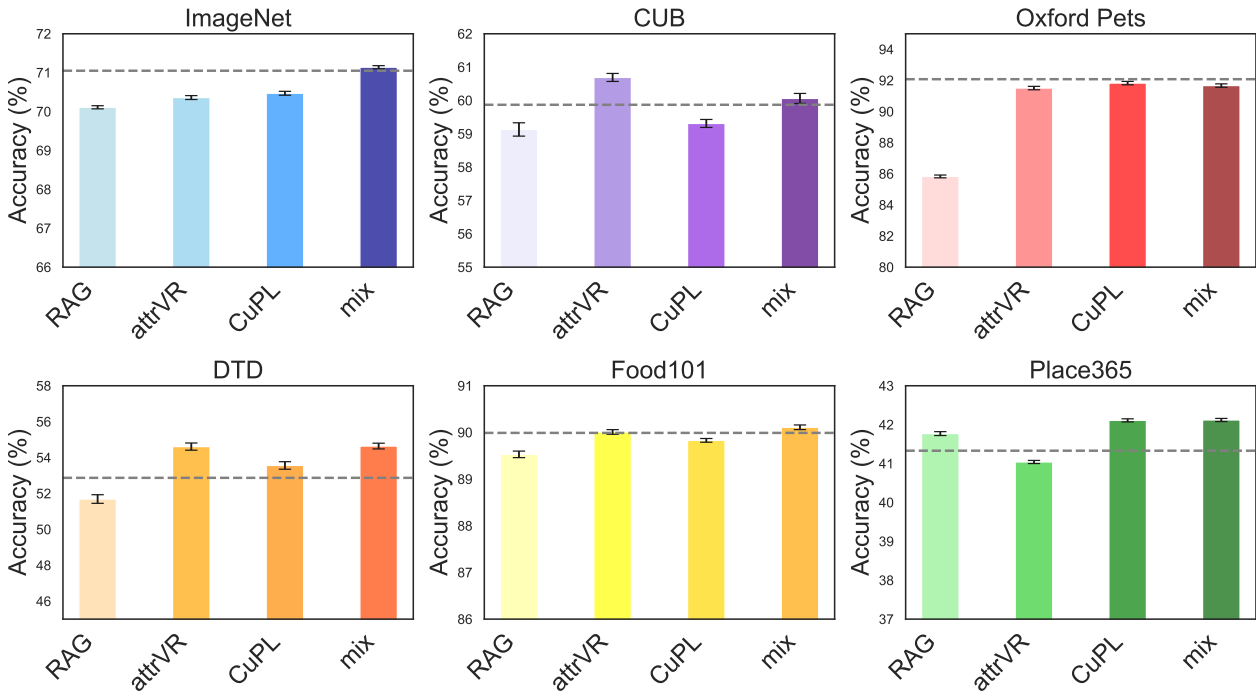

Figure 8: Results of exploring textual description studies, using the results of CLIP (B/16).

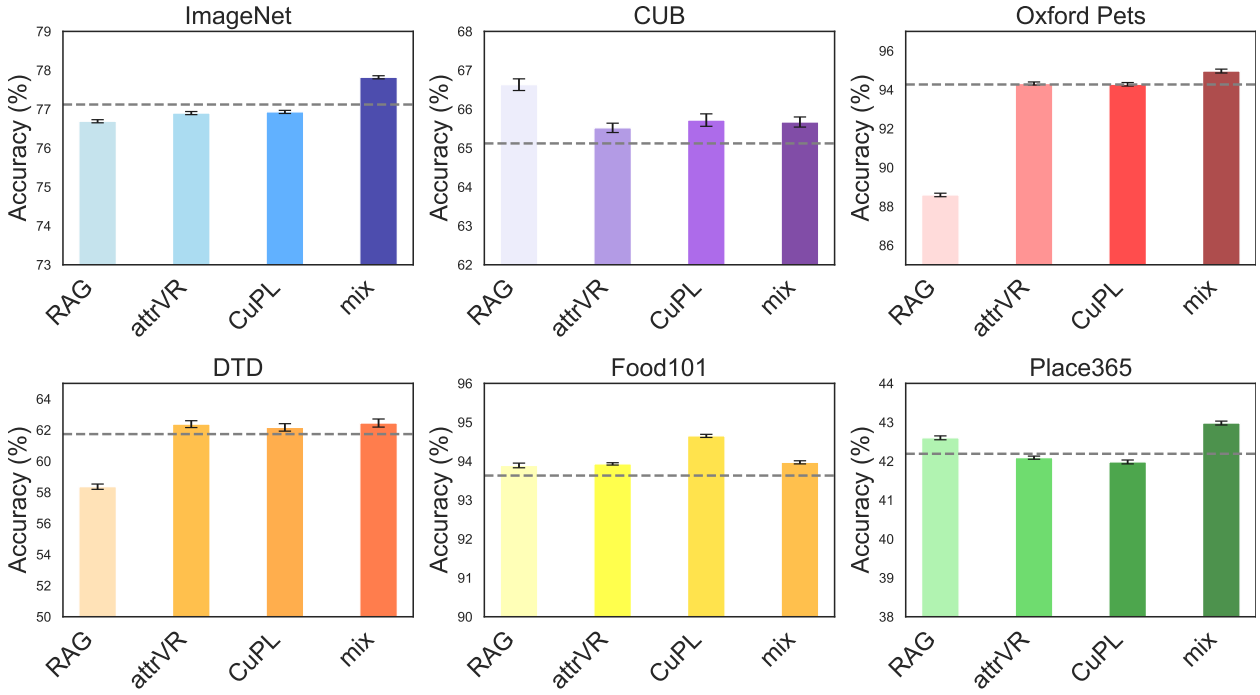

Figure 9: Results of exploring textual description studies, using the results of CLIP (L/14).

F Appendix 6: Limitation

One potential limitation we observed is that the textual descriptions generated by the LLM do not consistently focus on local features of the object. These descriptions often tend to be generic, making it difficult to associate specific parts of the text with corresponding local image patches from a human perspective. To address this, we aim to explore more advanced approaches to generate precise and localized descriptive texts that better align with the visual details of an image.